Small-scale magnetic alginate robots for localized antibiotic *E. coli* infection treatment

*Arnima Shrestha[1], Aarya Bandi[1], Noura Abdelrazec[1], Sirshendu Misra[2], Kartar Singh[3], Michael A. Beazely[3], Sushanta K. Mitra[2], Veronika Magdanz[1]**

A. Shrestha, A. Bandi, N. Abdelrazec, V. Magdanz
[1]Medical Microrobotics Lab, Waterloo Institute for Nanotechnology, Department of Systems Design Engineering, University of Waterloo, 200 University Ave W, Waterloo, Ontario N2L 3G1, Canada

S. Misra, S. K. Mitra
[2]Micro & Nano-Scale Transport Laboratory, Waterloo Institute for Nanotechnology, Department of Mechanical and Mechatronics Engineering, University of Waterloo, Waterloo, Waterloo, Ontario N2L 3G1, Canada

[3]K. Singh, M.A. Beazely**,** School of Pharmacy, University of Waterloo, 10A Victoria St. S. Kitchener, Ontario N2G 1C5, Canada

E-mail: veronika.magdanz@uwaterloo.ca

Keywords: small-scale robots, magnetic, antibiotics, norfloxacin, urinary tract infections

Abstract

Urinary tract infections are the most common infections worldwide and are typically treated with oral antibiotics which are distributed systemically, potentially leading to undesirable side effects such as allergies, disruption of the gut microbiome and increased antibiotic resistance. These challenges are further exacerbated in recurrent or chronic infections, where repeated use of broad-spectrum antibiotics is common. Strategies to avoid the worsening of antibiotic resistance include replacing systemic antibiotic treatment with local drug administration. For these reasons, a delivery strategy that provides drug administration at the disease site through active, wireless transport is urgently needed to improve urinary tract infection treatment. Wirelessly navigated small-scale, flexible robots have the potential for highly localized drug delivery and minimal invasive interventions. In this study, we present alginate-based flexible small-scale magnetic robots for localized antibiotic treatment of urinary tract infection. We

show that bacterial infection is rapidly cleared out from urine with the help of localized norfloxacin release from the robots. Magnetic navigation and real time ultrasound imaging of the alginate robots inside a pig urinary tract demonstrate the feasibility of implementation for localized noninvasive treatment. The proposed small-scale robots promise potential benefits such as localized drug action avoiding systemic drug distribution and side effects of conventional oral administration.

1. Introduction

Urinary tract infections (UTIs) are among the most prevalent bacterial infections worldwide, affecting approximately 150 million people annually and placing a significant burden on healthcare systems.[1] In the United States specifically, UTIs known to be one of the most common outpatient infections, leading to 8.6 million healthcare visits and an estimated cost of 1.6 billion dollars. UTIs commonly occur when uropathogens (most frequently *Escherichia coli*) from fecal flora ascend from the urethra to infect the bladder. Moreover, women are particularly susceptible to UTIs due to having a shorter urethra length, recurrent vaginal colonization and complete bladder emptying from prolapse and urinary retention.[2] Approximately 70% of women will be diagnosed with an UTI in their lifetime, and 30% of those will suffer from recurrent UTIs.[3] The symptoms of UTIs can vary in severity, as the infection can either be asymptomatic or symptomatic. These symptoms widely range from mild irritative voiding to bacteremia, sepsis or fatality.[4] Currently, the conventional strategy of treating UTIs is oral antibiotics administration, which can present a variety of side effects, which include diarrhea, nausea and vomiting, dizziness, rash, and yeast infections.

Several challenges of the current UTI treatment exist: 1) oral antibiotics administration causes systemic side effects such as gut microbiome alteration which is linked to antibiotic resistance,[5] 2) recurring or chronic urinary tract infections lead to the indiscriminate use of broad-spectrum antibiotics which further increases the prevalence of antibiotic resistance,[6] 3) oral antibiotic treatment is ineffective in patients with antibiotic resistance or intolerance. Strategies to avoid the worsening of antibiotic resistance include the prevention of infections whenever possible, and to replace systemic antibiotic treatment with local drug administration. People of particular risk are patients requiring long-term catheters or undergoing frequent surgery, and immunocompromised people.[7–9] The high prevalence and recurrence of UTIs urges the development of more targeted and effective treatment with lower side effects and less invasiveness avoiding recurrence and prolonged drug administration. Particularly for patients

with chronic UTIs, the current methods of persistent drug treatment are unsatisfying solutions that bring a huge burden to patients and healthcare systems.

For these reasons, a delivery strategy that provides drug administration at the disease site through active, wireless microrobots is urgently needed to improve urinary tract disease treatment.

To stall side effects of antibiotics treatment and stop increase of antibiotic resistance, an alternative to oral treatment is needed to circumvent the effects on the gut microbiome, the main driving factor of antimicrobial resistance.[10] Instead of relying on systemic methods, such as oral administration of antibiotics, microrobots have been proposed as a novel non-invasive method of achieving targeted local treatment.[11] Wirelessly navigated microrobots have been proposed for highly localized drug delivery and minimal invasive interventions thanks to their small size, remote control and non-invasive action.[11–14]

Research in microrobotics has been rapidly increasing due to their potential use in biomedical applications, which include targeted cargo delivery, minimally invasive surgery, diagnostics, and other in vivo applications. Microrobots can be driven by different actuation strategies, which include magnetic fields, electrical fields, light fields, thermal fields, chemical actuation and biological actuation.[15] The most promising approach for propulsion and control of such small-scale robots for minimal invasive interventions are low frequency rotating magnetic fields, thanks to their excellent penetration through tissues, their safety for humans, and compatibility with clinical settings.[15–17]

Several groups have proposed microrobots for the treatment of bacterial infections[18–20] due to the robot's abilities to disrupt biofilms, one of the strategies of bacteria's resistance, by actively disrupting biofilms with their motion[21], or releasing antibacterial chemicals. Microrobotic breakdown of biofilms in tissue infections have been demonstrated by production of antibacterial chemicals such as nitric oxide, reactive oxygen or nitrogen species.[22–25] Photoacoustically active or light-triggered microrobots have been shown to eliminate bacterial infections by irradiation.[26,27] Antibacterial microrobots have also been suggested for fighting implant[28] and tooth[29–31] infections with mechanochemical strategies.

Many of these strategies are promising, yet certain challenges for their implementation in medical interventions remain. Small scale robots need to be precisely navigated to guarantee controlled deployment and retrieval, and the localized action at the target site. A safe retrieval, or alternatively local degradation into nontoxic components needs to be implemented. The robots need to be imaged in real time in vivo and tailored to perform the desired medical task. Flexibility of microrobots offers specific benefits such as gentle interaction with soft tissue and

cells without mechanical damage and the ability to squeeze through tight spaces by changing their shape,[12] both crucial for biomedical applications.

In a recent study, the feasibility of using small-scale flexible hydrogel filaments for medical applications in the urinary tract was demonstrated.[32] A millimeter-sized enzyme-loaded filament was successfully navigated inside 3D printed human urinary tract models with the help of rotating permanent magnets and under real-time ultrasound imaging of the robots. The robots showed to significantly reduce the size of acid stones within days, suggesting this might be a feasible approach for localized, wireless treatment of urological diseases.

In this study, we aim to address the limitations of conventional UTI treatments by developing wirelessly navigated, small-scale alginate-based flexible robots for localized drug delivery. Alginate is a polysaccharide which is derived from brown seaweed and is well established material for controlled drug delivery.[33] Alginate has a polymer structure composed mainly of mannuronic and guluronic acids linked through 1-4 bonds and arranged in linear unbranched chains. Furthermore, sodium alginate, which is water soluble, can quickly form hydrogen bonds when crosslinked with multivalent cations such as Ca^{2+}.[34] Alginate has widely been used for drug loading and release,[35] for instance as norfloxacin-loaded microbeads.[36] Here, we demonstrate a facile approach toward utilizing alginate-based small-scale robots for UTI treatment. Alginate is used as the main structural material for its flexibility, nontoxicity, and easy loading of the antibiotic drug. Flexible alginate filaments with embedded micromagnets are fabricated using a simple, scalable, and reproducible mold-casting approach, which were subsequently loaded with the antibiotic via immersion-driven physical absorption. We leverage the magnetic interaction between an externally applied rotating magnetic field and the embedded micromagnet to control and propel these small-scale robots, ensuring precise drug administration directly at the infection site. The proposed application of soft, antibacterial small-scale filaments addresses several challenges of the conventional UTI treatment discussed above. The filaments are designed to navigate through the human urinary tract, and locally clear out bacterial infections caused by *Escherichia coli (E.coli).* An approach that is clinically relevant for localized antibiotic delivery utilizing magnetically navigated alginate-based microrobots enables a platform for drug release directly at an infection site while systemic exposure is minimized and therapeutic efficacy is improved.

2. Results and Discussion

2.1 Fabrication of small scale norfloxacin-loaded alginate filaments

3D printed negative molds (**Figure 1Ai**) were prepared to fabricate positive PDMS mold casts (Figure 1Aii) as templates for the crosslinking of alginate filaments with dimensions of 1x1x12 mm^3 with single 500x700 µm disc-shaped axially magnetized micromagnets (Figure Aiii) placed in the head position inside the mold. The alginate solution was cast into PDMS molds containing embedded micromagnets and subsequently crosslinked by immersion in 1.5% (w/v) calcium chloride solution to form stable filaments. After crosslinking, the filaments were released from the molds by tweezers (see resulting filaments in Figure 1Aiv). The average filament length, diameter and volume was measured to be 12.23±1.03mm, 1.25±0.22mm and 9.68±2.36mm^3, respectively, as determined by ImageJ analysis in x, y and z direction (n=12 filaments). The filaments are designed with micromagnet in a magnetization axis perpendicular to the long axis of the filaments (see Table of Content Graphic). This allows the filaments to align along external permanent magnets for helical forward propulsion (Figure 1Av). The motion of such magnetic filament is demonstrated in Supporting Information Video S1, showing the propulsion of the filament inside an aqueous solution in real time under 8 Hz magnetic rotational frequency.

It is known that drug loading capacity depends on a hydrogel's crosslinking density and pore size.[35,37] Hence, the physical absorption-driven drug loading of norfloxacin (NF) into the filaments was studied by fabricating filaments from three different concentrations of alginate (30, 35 and 40 mg/mL) and measuring the uptake of NF over time with spectroscopic analysis of the supernatant. Figure 1Bi shows the uptake of NF into the alginate filaments over 24 hours at pH7, demonstrating a saturation of NF concentration inside the filaments after about 15 hours. The concentration of alginate in the loading solution does not have a significant effect on the loading capacity, as the final loading amount of NF is 0.25 mg/mL NF per filament.

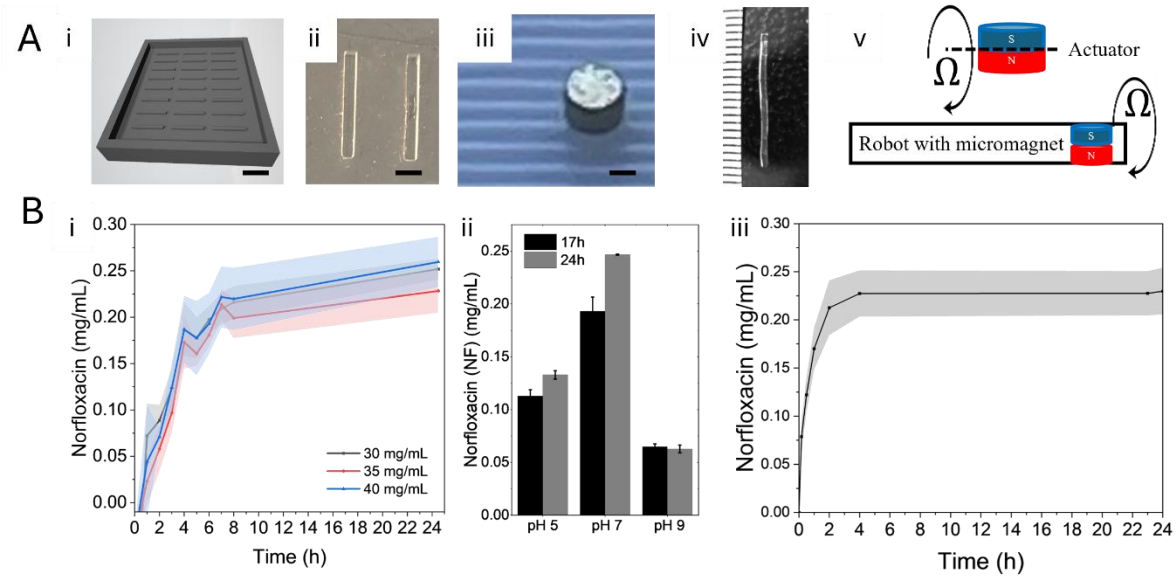

Figure 1. A) Alginate filament fabrication. i)3D printed negative mold. Scale bar: 10mm, ii) PDMS mold for alginate filaments, Scale bar 2 mm, iii) 500x700µm axially magnetized micromagnet (scale bar: 200µm) to be embedded in iv) alginate filaments. Scale bar 2mm. v) Magnetic configuration of actuator and robot magnet. Bi) Norfloxacin (NF) loading amount into alginate filaments with 30, 35 and 40 mg/mL alginate concentration over 24 hours at pH7. Bii) NF loading amount inside alginate filaments depending on pH of NF loading solution tested at 17h and 24h. Biii) NF release from NF-loaded filament over 24 hours at pH7 in synthetic human urine. Shaded areas indicate the standard deviation(n=9).

Human urine can vary in pH from 4.5-8.5, [38] which can impact the release kinetics of the drug, as it is known that alginate is pH-dependent. After alginate gelation, water molecules are physically entrapped inside the alginate matrix, but are still free to migrate, which contributes to the utilization of alginate in many applications such as cell encapsulation and drug delivery.[35] The pH affects the pore size and swelling state of the alginate gel, ultimately determining the loading and release ability of the material. For this intended application in the human urinary tract, the loading capacity of the alginate filaments was tested in pH 5, 7 and 8 of synthetic human urine (Fig. 1Bii). As expected, there is a strong pH dependence of the loading capacity, with the maximum loading amount of 0.25 mg/mL detected at pH7, compared to 0.12 mg/mL at pH 5 and 0.05 mg/mL at pH 8. The NF release kinetics of the alginate filaments were investigated and the amount of NF released over time at pH 7 is displayed in Figure 1Biii.Within two hours, more than 85% of the antibiotic is released, and close to 100% of drug release is completed within 24 hours. A rapid release of antibiotics is desired to have an immediate killing effect of the bacteria in the surroundings of the filament.

2.2 Magnetic propulsion of filaments

The embedded micromagnets in the alginate filaments allow the navigation inside *in vitro* bladder, ureter and renal pelvis phantoms, similar to previously reported gelatin-based urease-

containing filaments used for local kidney stone dissolution.[32] The micromagnets respond to external rotating magnetic fields by a screw-like forward motion of the flexible alginate filament, as shown in Video S1 and in image series in **Figure 2**A. The actuation is generated by a previously reported actuation system consisting of a external permanent magnet (Neodymium-iron-boron, N52, 523 mT surface magnetic field strength) rotated by a DC motor and held by a IGUS 4 degree-of-freedom robot arm.[32,39] The motion mechanism and actuation setup of these flexible millimeter-sized robots was described previously.[40] At a distance of 5 cm from the robot, the actuator generates a field strength of 7 mT. The robot aligns its magnetization axis (which is perpendicular to the robot's long axis) continuously with that of the actuator magnet, leading to a screw-like forward motion**. Figure 2B** summarizes the average robot velocities obtained under influence of external rotating magnetic fields. The robot velocity increases with rising rotational frequency of the actuator magnet, reaching a constant speed of 11 mm/s (approximately one robot bodylength per second) at frequencies above 12 Hz (**Figure 2B**).

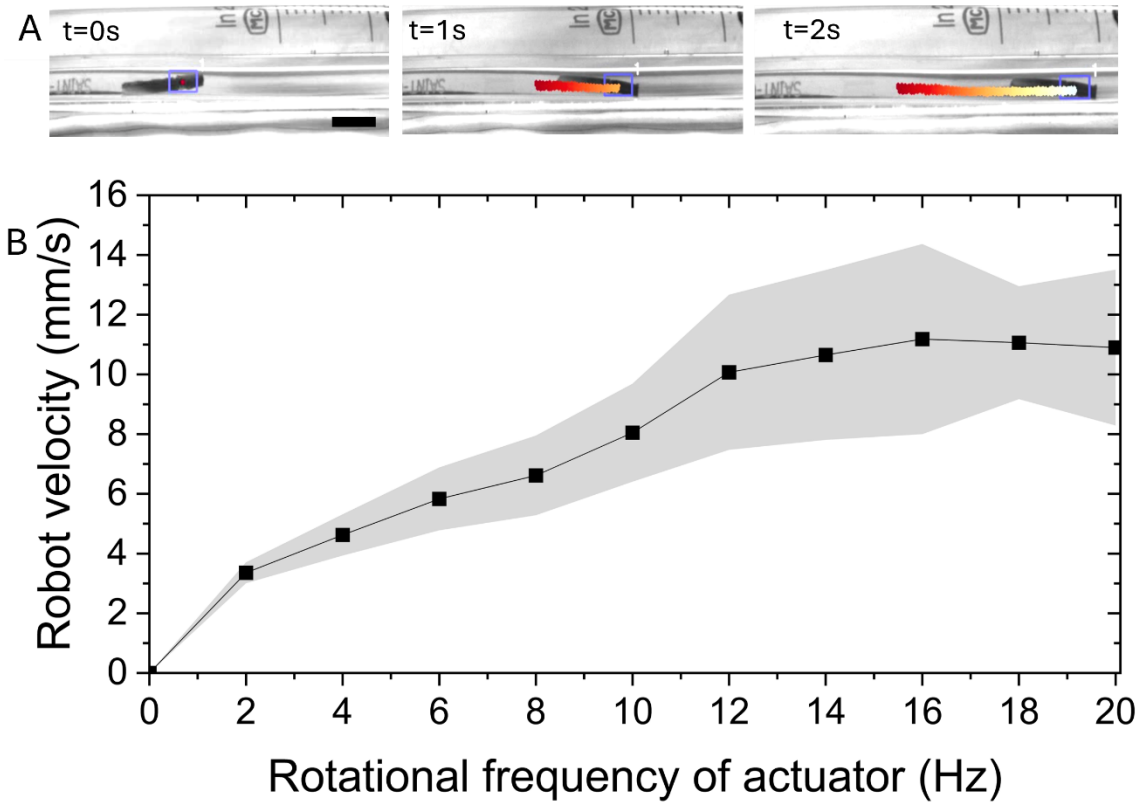

Figure 2: Magnetic propulsion of a flexible alginate filament robots. A) Image series of alginate filaments moving under influence of rotating magnetic field at actuator frequency of 10 Hz inside a silicon tube mimicking the ureter anatomy with an inner diameter of 6 mm. The filament was stained with food colour to increase contrast of the alginate. A tracking software is used to measure robot forward velocity and display the trajectory and image series with a coloured track. Slight deformations of the filament hint to the flexible motion of the robot. Scale bar is 5 mm. B) Average robot velocities depending on actuator frequency obtained from 10 alginate robots for each frequency response. The

grey shade displays the standard error of the mean of the robot velocities. See also Video S1 of an alginate filament robot moving at 8Hz actuator rotational frequency.

2.3 Norfloxacin-loaded magnetic filaments inhibit *E.coli* growth

The effect of norfloxacin-loaded alginate filaments was tested on *E.coli*-infected synthetic human urine that mimics a urinary tract infection in terms of *E.coli* concentration and composition of the medium. *Escherichia coli* is the bacteria causing most UTIs.[41] The composition of human synthetic urine was adapted from Brooks et al.[42] recommended for growth of urinary pathogens. The initial inoculation of urine with *E.coli* was set to about $5x10^7$ cells/mL, which corresponds to a typical amount of *E.coli* found in an acute UTI.[41]

The norfloxacin-loaded filaments were compared to the effect of pharmacological levels of norfloxacin that would result from oral administration of norfloxacin during conventional UTI treatment. An average daily dosage of 400 mg norfloxacin resulted in serum concentrations of 1.35 to 1.58 mg/L NF within 1-2 hours.[43] An increase above 800 mg per day did not increase NF serum concentration beyond this average. Approximately 30% of any oral NF dose is typically excreted as norfloxacin into the urine[43]. Considering an excretion dosage similar to serum of 1 mg/L (i.e. 1 µg/mL), we chose a final control concentration of 10 µg/mL NF in urine as a resulting upper limit of NF in conventional oral administration for UTI treatment.

We compared the *E.coli* growth in urine over 120 hours at 37 degrees Celsius across the different samples (see **Figure 3**): 1) an untreated *E.coli*-inoculated urine sample (control), 2) *E.coli*-inoculated urine injected with 10 µg/mL norfloxacin to mimic an oral systemic antibiotic treatment (NF Solution), 3) inoculated urine containing an alginate filament without any antibiotics (Alginate Filament), and 4) a NF-loaded alginate filament immersed in the inoculated urine (NF loaded Alginate Filaments) (see **Figure 3**). Panel A in **Figure 3** displays illustrative scanning electron microscopic images of the urine after 120 hours of incubation at 37ºC, with the alginate filament visible in **Figures 3Aii** and **3Aiv.** While the untreated control sample in Ai shows a large accumulation and growth of *E.coli* bacteria in the urine, less bacteria were observed in **Figures 3Aii-Aiv**. The reduction in bacterial growth in samples containing NF and NF-loaded filaments can be contributed to the direct effect of the antibiotic. Surprisingly, the sample with the control alginate filaments (no NF) also showed reduced bacterial growth at 120 hours compared to the control(**Figure 3Aiii** and B), suspecting an antimicrobial activity by the calcium alginate directly as reported in the literature[44,45], or an absorption of bacteria into the filaments, reducing the bacteria in suspension.

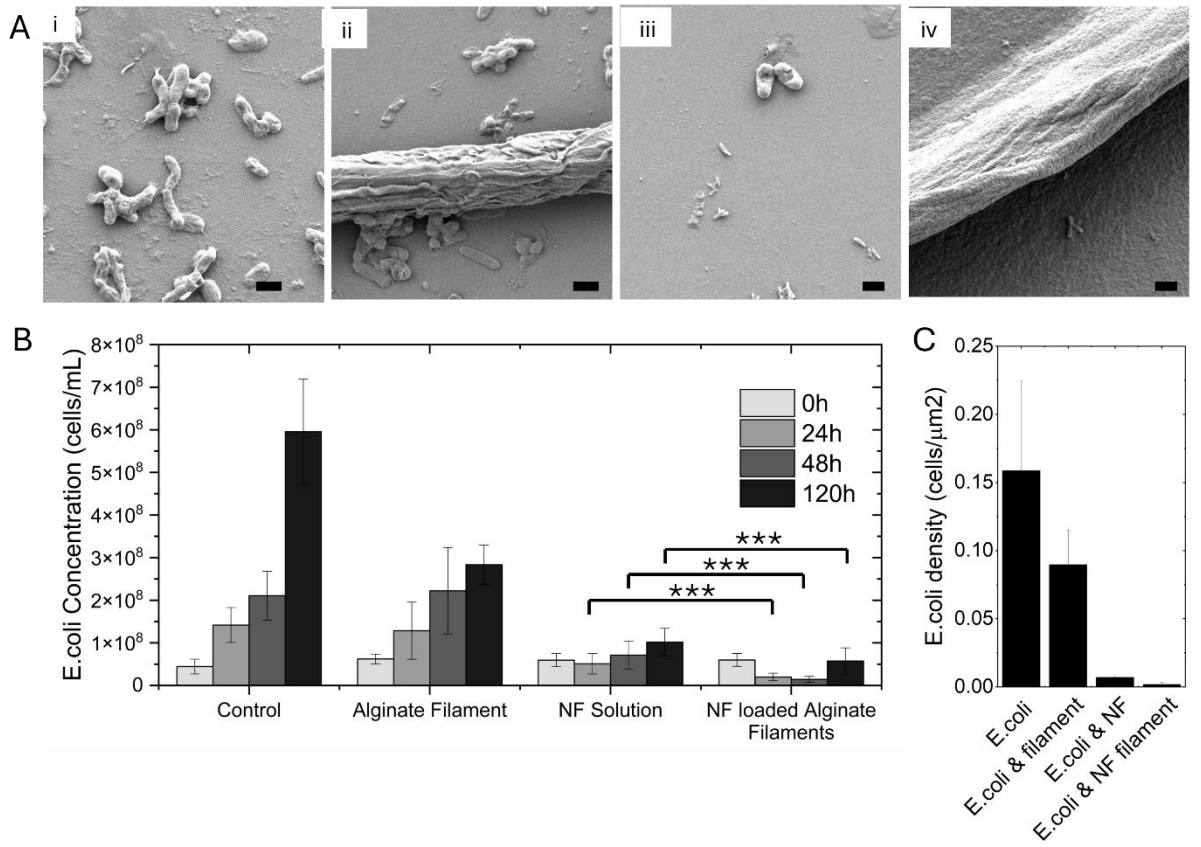

Figure 3: Effect of Norfloxacin-loaded filaments on *E.coli* infected human synthetic. A) Scanning electron microscopy images of *E.coli*-infected urine after 120 hours of incubation. *E.coli*-infected urine with Ai) no additives (control), Aii) alginate filament (no antibiotic), Aiii) treated with 10 µg/mL Norfloxacin, Aiv) treated with Norfloxacin-releasing alginate filaments. Scale bars are 2 µm. B) Average *E.coli* concentration (with standard deviation as error bars) in synthetic urine measured by optical density at 600nm over cultivation period of 120 hours at 37 ºC without additives (control), unloaded alginate filaments, NF solution (norfloxacin addition of 10 µg/mL at 0h), and NF loaded alginate filaments (norfloxacin-loaded alginate filaments). Detailed statistical results are included in **Table S1**. C) *E.coli* bacterial density after 120 hours determined from fixated droplets of each sample, as detected in scanning electron microscopic images in A). Error bars are standard deviations from 3 analyzed images per sample.

Analysing the bacterial growth across the different samples obtained from triplicate well readings performing 3 - 5 repeated experiments (a total of n=12 readings or more per condition), it is evident from **Figure 3B** that most efficient *E.coli* growth inhibition was achieved in samples containing the NF loaded alginate filaments, reducing the bacterial infection from $5x10^7$ cells/mL within 24 hours to $2x10^7$ cells/mL , while the control samples show increase of bacterial growth to $1.4x10^8$ cells/mL (inoculated urine (control)) and $1.2\ x10^8$ cells/mL (alginate filaments). The NF loaded alginate filaments also significantly outperform the antibiotic injected urine, in which the bacterial growth is inhibited, but maintains the same level after 24h with $5x10^8$ cells/mL. After 48h, the NF loaded alginate filaments have reduced the *E.coli*

concentration to $1.4x10^7$ cells/mL, again performing better than directly injected antibiotic ($7x10^7$ cells/mL at 48h for NF solution). After 120 hours, the bacterial concentration of the NF loaded alginate filaments sample equals $5x10^7$ cells/mL, which corresponds to the initial bacteria concentration. This means, bacterial growth was suppressed completely by the NF-releasing filaments across the 120 hour timeline, with strongest inhibition in the 24-48 hour range, corresponding to the release profile shown in **Figure 1Biii**. A 68% growth of *E.coli* was observed in the sample injected with 10 µg/mL NF over 120h incubation compared to the initial bacterial concentration. A bacterial growth of 350% was observed in the sample containing alginate control filaments, and 1238% in the control sample, indicating exponential bacterial growth in the urine, typical for untreated bacterial infection. These results indicate that the sustained release of antibiotic from the filament shows superior efficacy compared to the systemic approach of one-time antibiotic addition to the urine, particularly on after 24 and 48 hours visible by strongest bacterial growth inhibition in that time period. Statistical analysis indicates the significantly improved bacterial growth inhibition across the 120 hour timeline (see **Table S1**) by the NF-loaded filaments. The significantly reduced bacterial cell density was also observed on scanning electron images taken after 120 hours of incubation time (**Figure 3C**).

2.4 Viability of HEK kidney cells in presence of alginate filaments

Toxicity of the robotic filaments was investigated by coculture of alginate filaments with human kidney cells (HEK-293). Viability stains of the kidney cells were performed after 48 and 120 hours with a live/dead stain (see **Figure 4**). The HEK culture was inoculated with bacteria to mimic a bacterial infection in the renal pelvis. Control samples (**Figure 4Ai** and **Aii**) show little kidney cell growth, inhibited by the presence of bacteria. Samples with administesred NF and NF-loaded alginate filaments recovered HEK growth to 30% and 70% confluence within 120 hours (See **Figure 4Aiii** and **Aiv**). Overall cell viability was equivalent to the control, showing 100% cell viability, indicating no toxic effects caused by the NF-loaded alginate filaments.

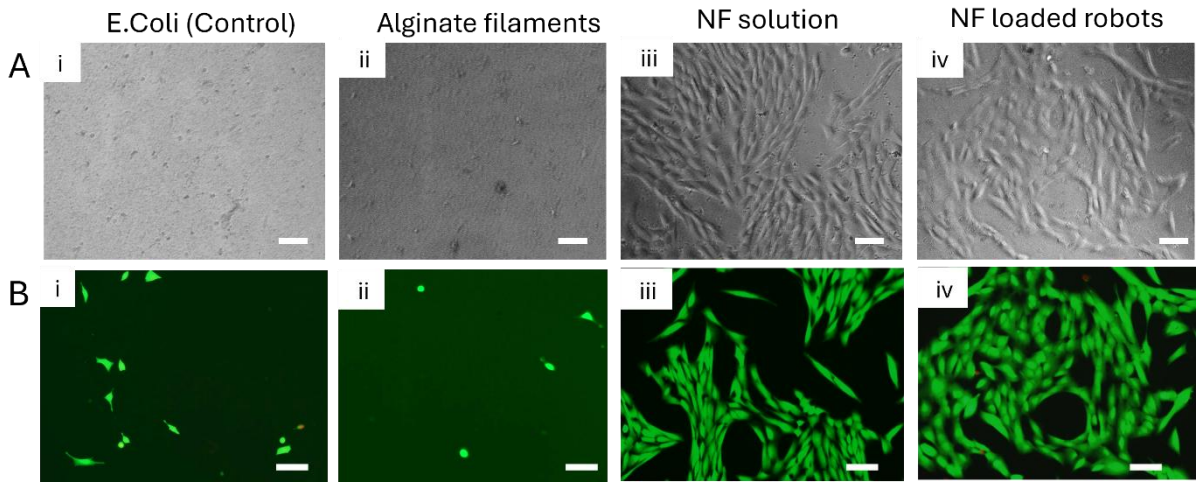

Figure 4: Cytotoxicity test of antibiotics loaded filaments on human embryonic kidney cells (HEK). Live/Dead viability stained human embryonic kidney cells (HEK) incubated in infected culture medium for 120 hours. A) Brightfield and (B) fluorescent images of live (Calcein-stained green) and dead (Propidium iodide stained red) cells i) Control (no filaments), ii) with alginate filaments, iii) with NF injection, iv) with NF-releasing alginate filaments.Scale bars are 100 µm.

2.5 Navigation and real-time imaging of alginate filaments in ex vivo porcine urinary tract

To demonstrate the feasibility of wireless navigation of these alginate bots inside the urinary tract, *ex vivo* experiments were performed on porcine urinary tract, an established model system for surgical training and treatment methods.[46,47] The upper porcine urinary tract is very similar in anatomy and size to the human system and is therefore commonly used as model system. Fresh porcine kidneys with intact ureters were obtained as donations from a local slaughterhouse and transported to the lab immediately. The ureters were catheterized with a 14 French catheter which was connected to a syringe with 50 ml SHU (**Figure 5A**). Kidney and ureter were filled with SHU through the catheter. Then, an alginate filament robot was introduced into the catheter and guided into the ureter with external magnetic actuation at 2Hz (**Figure 5B**, Video S2). The actuator was handheld at a distance of 5-15cm parallel to the robot (**Figure 5C**).

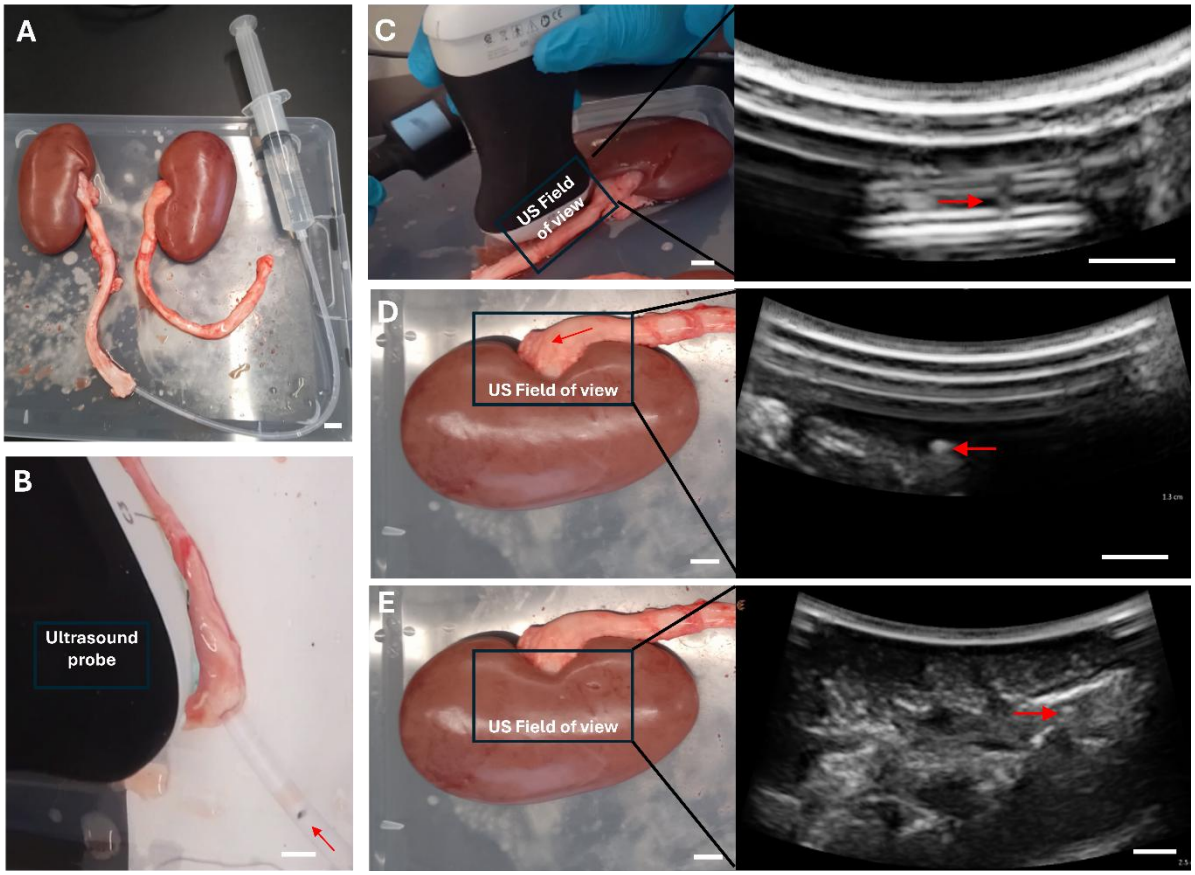

Figure 5: Ex vivo navigation and real-time ultrasound imaging of magnetic alginate filaments inside porcine urinary tract. A) Porcine ureter was catheterized with 14 French catheter and filled with synthetic human urine. B) Robot deployment:A Clarius ultrasound probe was handheld on the surface of the extracted organ for real-time imaging once robot entered ureter. (Video S2) C) External magnetic navigation by handheld rotating permanent magnet (left), while imaging the robot inside the ureter by ultrasound. The ultrasound image on the right is extracted from the imaging livestream (see supporting video S3). The red arrow points at the signal obtained from the embedded micromagnet inside the filament. D) Robot navigation into the uteropelvic junction. The black box indicates the field of view used for the ultrasound probe with real-time image on the right. The bright signal is obtained from the micromagnet inside the filament. (supporting video S4) E) Navigation and ultrasound imaging inside the renal pelvis. The ultrasound image illustrates the branched channels inside the kidney, with the bright spot indicating the location of the robot. Scale bars are 5 mm. See also supporting information video S5.

Once the robot entered the ureter through the catheter, it was continuously propelled by the externally rotating magnet, while being imaged in an ultrasound livestream (see Figure 5C and supporting information video S3). The ultrasound probe imaging enables sufficient contrast-to-noise ratio to continuously detect the robot location inside the organ. The good signal is obtained thanks to the good echogenicity of the Neodymium micromagnet, and also thanks to the rotating motion of the robot, which can be easily recognized in the ultrasound livestream (see videos S3-S5 in supporting information). From the ureter, the robot was continually guided by the external actuator into the uteropelvic junction (**Figure 5D**), which is the curved entrance into the kidney (video S4). The actuator was held parallel to the robot location at a distance of about 10 cm, and was not used to attract the robot in any direction to avoid it from getting stuck, but solely to align the robot's long axis along the rotating axis for forward propulsion. Throughout the entire experiment, no adhesion of robot to tissue was observed, and continuous rotation of the robot inside the ureter, uteropelvic junction and kidney (**Figure 5E**) (see

supporting information video S5) was achieved, as indicated by a constant flickering of the robot signal in ultrasound. After successful guidance of the robot into the renal pelvis, the actuator was placed above the uteropelvic junction and the robot was retrieved from the opening. This experiment shows feasibility of real-time imaging of the robots, successful robot deployment and retrieval and magnetic guidance in a real organ.

3. Conclusion

In this study, we demonstrate a proof-of-concept for the localized treatment of bacterial urinary tract infections with the help of wireless, magnetic small-scale robots. We demonstrate the fabrication of alginate-based flexible filament robots with embedded micromagnets which provide magnetic response to external rotating magnetic fields. The loading of norfloxacin, a model antibiotic targeting *E.coli* infections, allows for the localized release of antibiotics at the site of infection. The bacterial growth study presented here highlights the benefits of the controlled antibiotics release with effective *E.coli* growth inhibition in synthetic human urine. A high cargo load of 250 µg per filament was achieved, which is sufficient to supress bacterial growth significantly over several days, while also being significantly lower than conventional oral daily antibiotics dosage. It is evident that oral administration requires much higher dosage, e.g. a standard of 800 mg / day, whereas the here presented method delivering 0.25mg of antibiotics in a concentrated fashion to the infected urine can manage to control bacterial growth with up to 3200x lower dosage, depending on the urine volume.[43,48] This highlights the potential reduction of antibiotics usage with localized delivery and controlled release of the drug for enhanced infection treatment. The direct comparison of the presented active delivery and release approach with conventional method of oral administration remains to be investigated.

The approach presented here—using millimeter-sized alginate robots for urinary tract infection (UTI) clearance—is unique in its ability to deliver effective antibiotic doses that successfully inhibit bacterial growth in urine. These robots were also demonstrated to be magnetically guided and imaged inside real organs in real time using ultrasound, capabilities that have not previously been reported in this context. Compared with other micro- or nanorobotic strategies for infection treatment, this platform offers significant advantages due to its high drug-loading capacity and rapid delivery to the infection site, which is critical for timely treatment of UTIs. In contrast, most nano- or microscale robots reported to date focus on mechanical or chemical biofilm disruption, often relying on the generation of antibacterial free radicals—mechanisms that are not the primary therapeutic strategy for UTI treatment.

The discussion does not adequately contextualize the work within the broader field of microrobots for infection treatment. For example, how do the alginate robots compare to other magnetically driven systems (e.g., biofilm-disrupting microrobots or nitric oxide-releasing designs)? A comparative analysis of loading capacity, actuation efficiency, and antibacterial performance would highlight the novelty of this approach.

The ex vivo navigation and ultrasound imaging of these robots inside a pig urinary tract demonstrate the feasibility for minimally invasive procedures. The deployment and retrieval of the robots can be achieved through standard 14 French catheter (4.7mm in outer diameter). Propulsion of the robots inside the ureter and kidney did not pose any major challenges and robots were visualized ultrasound in real-time the entire time of magnetic navigation inside the organs. No adhesion to the tissue or loss of control was encountered throughout the experiment. Further studies are needed to investigate the deployment and retrieval of the proposed robots through urinary catheterization of the bladder, and navigation and imaging inside the urinary tract in living animals and humans once appropriate approvals can be obtained. Our recent study on imaging of small-scale robots in X-ray fluoroscopy[49] and ultrasound[32] in ex vivo models suggests that simultaneous robot imaging and navigation is possible in real time against blood flow. Additional experiments are needed to investigate the robot navigation against urine flow and peristaltic motion of the ureter. These biopolymeric flexible robots are designed in size that they can remain inside the renal pelvis for several days and can be flushed out through the urinary tract upon completion of treatment. The natural passing of the robots need to be confirmed. Alternatively, magnetic navigation can be used to retrieve th robots. Further, studies on any adverse effects in living organisms over elongated periods of time such as inflammatory responses, need to be conducted in the future.

Overall, this approach promises to make antibiotic treatment more targeted and effective, lowering overall required dosage and recovery time of the patient, offering a reduction in antibiotics usage. This contributes to a much-needed reduction in usage of antibiotics, promising to circumvent antibiotic resistance development. It could be a particularly interesting approach when combined with other microrobotic treatment applications such as kidney stone removal[32], where antibiotics administration is routinely performed.

4. Methods

Preparation of synthetic human urine (SHU)

Synthetic human urine (SHU) was prepared according to the recipe suggested for mimicking conditions of urinary tract infections[42] with minor adjustments. For 1 liter of SHU, 1g peptone, 0.005 g yeast extract, 0.1g lactic acid, 0.4g citric acid, 2.1g sodium bicarbonate, 10 g urea, 0.07 g uric acid, 0.8 g creatinine, 0.37 g calcium chloride, 5.2g sodium chloride, 0.49 magnesium sulfate heptahydrate, 3.2 g sodium sulfate, 0.95 g potassium phosphate, 1.2g potassium phosphate dibasic and 1.3g ammonium chloride were mixed in 1L milliQ water.

Magnetic actuation experiments

The magnetic actuation setup includes a robotic arm (igus Robolink) with a DC motor (brushed 24 volt DC motor, Maxon motor) attached to its end-effector. The motor facilitates rotational movement for a permanent NdFeB magnet with dimensions 1 x 2 inches, on which the surface field of the magnet is 5233 Gauss (0.5233T), Brmax is 14,800 Gauss (1.48T) and BHmax is 52 MGOe (416kJ/m3). The rotational speed of the actuator magnet is controlled by an Arduino Uno and a Motor Shield from Adafruit creating a range of frequency between 2 - 20 Hz. The robot motion was recorded with a Basler camera at 75 frames per second. The videos were processed using a python based algorithm (The Nano-micromotor Track
ing Tool (NMTT) https://github.com/rafamestre/NMTT-nanomicromotor-tracking-tool), facilitating tracking of the micromagnets inside the robots and calculating the average velocity of the robots. The output of the code gives the total displacement of the robot and duration of motion. The analysis of motion was performed by a similar Python-based tool (Nano-micromotor Analysis Tool (NMAT) https://github.com/rafamestre/NMAT
nanomicromotor-analysis-tool), providing the average speed of the filaments based on data gathered from the NMTT.

Fabrication of magnetic small-scale alginate filaments

To create a 30 mg/mL alginate solution, 0.45 g of alginic acid sodium salt from brown algae was dissolved in 15 mL of MilliQ water at 55°C and 400 RPM using a magnetic stirrer. The alginate powder was added gradually to prevent clumping. Once fully dissolved, the alginate solution was transferred to a 15 mL centrifugation tube and centrifuged for 3 minutes at 300 RCM and 25°C. The solution was then pipetted into PDMS molds (1x1x10mm^3) to form filaments. The alginate filaments were submerged in a 1.5% $CaCl_2$ solution for 5 minutes, then removed with tweezers and immersed in the same solution for an additional 10 minutes. Afterward, the filaments were stored in water.

Fabrication of Norfloxacin Loaded Alginate Filaments

A Norfloxacin stock solution (5 mg/mL) was prepared by sonicating 10 mg of Norfloxacin (Sigma-Aldrich N9890) in 2 mL of Dimethyl Sulfoxide. This stock solution was diluted with MilliQ water to create a 0.5 mg/mL Norfloxacin solution. The pH of the 0.5 mg/mL solution was adjusted to 7 using 0.5M sodium hydroxide. 1 mL of the 0.5 mg/mL Norfloxacin solution was transferred to 1.7 mL graduated microcentrifugation tubes containing the alginate filaments. The tubes were wrapped with aluminum foil and incubated for 48 hours.

Norfloxacin Loading and Release

The loading and release of norfloxacin measured by absorbance measurements in a Tecan plate reader at 320 nm was correlated to Norfloxacin concentration by measuring the absorbance of a dilution series of Norfloxacin (0.25, 0.125, 0.625, 0.03125, 0.015626, 0.0078125 mg/mL) by linear regression[50].

E. coli Suspension preparation

We used *Escherichia coli* (K-12 Strain SMG 123, PTA-7555, ATCC, Cedarlane, Canada) for our experiments. The stock solution was prepared by incubating the bacterial sample in autoclaved Lauryl Tryptose (LT) broth (catalog no. DF0241170, Difco) in a shaking incubator (100 rpm) at 37°C for ~18 hours. The initial *E. coli* cell concentration in the stock solution was determined by cell counting using a hemocytometer. The desired *E. coli* cell concentration was prepared by diluting the bacterial suspension with SHU. The concentration of *E. coli* in SHU was then measured by optical density at 600nm in a 96 well plate in a Tecan plate reader.

Antibiotic E. coli treatment

The following samples were prepared in 1.5mL Eppendorf tubes with 1mL synthetic human urine at pH 7, inoculated with *E.coli* ($5.6 \pm 0.8 \times 10^7$ cells/mL) respectively: 1) without any norfloxacin (positive control), 2) 10 µg/mL NF addition at time t=0h (negative control), 3) addition of alginate filaments (containing no NF), 4) NF-loaded alginate filaments (loaded according to above procedure). The samples were incubated at 37 ºC for 120 hours. Optical density (Tecan Plate Reader) measurements of the supernatant were performed at 0h, 24h ,48h ,120 h at 600nm to measure the *E.coli* concentration in each sample.

Scanning Electron Microscopy

2.5% of glutaraldehyde was prepared from the 50% glutaraldehyde stock solution. 4 small pieces of silicon wafers were carefully cleaned with acetone and ethanol. On each silicon wafer, 10 µl of the following samples were added: 1) Control E. coli suspension, 2)E. coli suspension with the alginate filament, 3)E. coli suspension with the norfloxacin drug and 4) E. coli with the norfloxacin in the filament. Then 20 µl of the diluted glutaraldehyde solution was added to

the silicon wafers, where they were incubated for 1 to 2 hours at regular temperature wrapped with aluminum foil, to be protected from the light. After the fixation, the smear was immersed in 1x phosphate buffer and washed 3 times. Then each of the samples was washed sequentially in 50%, 70%, 95% and 100% ethanol (3 times). The samples were air dried at room temperature for at least 1 hour, and the samples were then dried overnight. The samples were covered with petri dishes to ensure that no dirt settled on the surfaces, and carbon tape was used to attach samples on SEM strands. In the following day, gold was sputter coated on the samples, and the samples were observed by using a scanning electron microscope.

HEK cell culture and cytotoxicity testing

HEK-293 cells (CRL-1573, ATCC, U.S.) were cultured in high glucose medium containing 10% fetal bovine serum and 1% Penicillin/Streptavidin in T15 flasks to confluence. Cells were released from the flask bottom by trypsinization and seeded into 24-well plates at a cell concentration of 50,000-10,000 cells/well. Viability stains were performed after 24 hours with Calcein AM and Propidium iodide staining and imaged with a Zeiss Axio Observer.

Ex vivo experiments

Pig urinary tracts were received as donations from Conestoga Meats (Breslau, Ontario) and immediately transported to the lab on ice. The ureters were filled with SHU via a 14 French catheter. Alginate filaments containing micromagnets were introduced into the catheter and navigated by external actuator at 2Hz constant rotation. A Clarius C3 HD3 wireless ultrasound scanner was used for real-time imaging of the robots throughout the whole experiments applying vascular or superficial mode. Videos were recorded and provided for review through the Clarius Cloud.

Statistical Analysis

Statistical Analysis of loading and release kinetics, E.coli cell concentrations, were performed by one-way ANOVA Tukey test in Origin software. Statistical indicators of *** (p-value < 0.001), ** (p-value < 0.01) , * (p-value < 0.05) and n.s. (p-value > 0.05) are noted in the plotted data. Unless noted otherwise, error bars and error shades are indicating the standard deviation.

Supporting Information

Supporting Information is available from the Wiley Online Library or from the author.

Acknowledgements

VM thanks the CBB seed fund and NSERC Discovery grant for financial support. VM and AS thank Nina Heinig and WatLab for support in SEM imaging. The authors thank Conestoga Meats for the kind donations, and Narenkrishna Thambidurai for assistance in ex vivo experiments.

Received: ((will be filled in by the editorial staff))

Revised: ((will be filled in by the editorial staff))

Published online: ((will be filled in by the editorial staff))

References

[1] A. L. Flores-Mireles, J. N. Walker, M. Caparon, S. J. Hultgren, *Nat. Rev. Microbiol.* **2015**, *13*, 269.
[2] C. M. Chu, J. L. Lowder, *Am. J. Obstet. Gynecol.* **2018**, *219*, 40.
[3] N. F. Abou Heidar, J. A. Degheili, A. A. Yacoubian, R. B. Khauli, *Urol. Ann.* **2019**, *11*, 339.
[4] B. Foxman, *Am. J. Med.* **2002**, *113*, 5.
[5] S. A. Kelly, A. M. Rodgers, S. C. O'Brien, R. F. Donnelly, B. F. Gilmore, *Trends Biotechnol.* **2020**, *38*, 447.
[6] R. Bartoletti, T. Cai, F. M. Wagenlehner, K. Naber, T. E. Bjerklund Johansen, *Inc. EAU-EBU Update Ser.* **2016**, *15*, 81.
[7] L. E. Nicolle, *Antimicrob. Resist. Infect. Control* **2014**, *3*, 1.
[8] R. Ramanathan, T. M. Duane, *Surg. Clin.* **2014**, *94*, 1351.
[9] Z. Tandogdu, T. Cai, B. Koves, F. Wagenlehner, T. E. Bjerklund-Johansen, *Eur. Urol. Focus* **2016**, *2*, 394.
[10] F. M. E. Wagenlehner, U. Hoyme, M. Kaase, R. Fünfstück, K. G. Naber, G. Schmiemann, *Dtsch. Arzteblatt Int.* **2011**, *108*, 415.
[11] P. Erkoc, I. C. Yasa, H. Ceylan, O. Yasa, Y. Alapan, M. Sitti, **2019**, *1800064*, 1.
[12] M. Medina-Sánchez, V. Magdanz, M. Guix, V. M. Fomin, O. G. Schmidt, *Adv. Funct. Mater.* **2018**, *28*, 1707228.
[13] L. Sonntag, J. Simmchen, V. Magdanz, *Molecules* **2019**, *24*, 3410.
[14] B. J. Nelson, I. K. Kaliakatsos, J. J. Abbott, *Annu. Rev. Biomed. Eng.* **2010**, *12*, 55.
[15] Z. Wang, Z. Xu, B. Zhu, Y. Zhang, J. Lin, Y. Wu, D. Wu, *Nanotechnology* **2022**, *33*, DOI 10.1088/1361-6528/ac43e6.
[16] N. Ebrahimi, C. Bi, D. J. Cappelleri, G. Ciuti, A. T. Conn, D. Faivre, N. Habibi, A. Hošovský, V. Iacovacci, I. S. M. Khalil, V. Magdanz, S. Misra, C. Pawashe, R. Rashidifar, P. E. D. Soto-Rodriguez, Z. Fekete, A. Jafari, *Adv. Funct. Mater.* **2021**, *31*, 1.
[17] J. J. Abbott, O. Ergeneman, M. P. Kummer, A. M. Hirt, B. J. Nelson, *IEEE Trans. Robot.* **2007**, *23*, 1247.
[18] W. Zhong, S. Handschuh-Wang, U. T. Uthappa, J. Shen, M. Qiu, S. Du, B. Wang, *ACS Nano* **2024**, *18*, 32335.
[19] X.-Y. Liu, R.-F. Li, J. Jia, Z.-L. Yu, *Theranostics* **2024**, *14*, 1029.
[20] Z. Zhang, L. Wang, T. K. F. Chan, Z. Chen, M. Ip, P. K. S. Chan, J. J. Y. Sung, L. Zhang, *Adv. Healthc. Mater.* **2022**, *11*, e2101991.

[21] L. Zhao, W. Li, Y. Liu, Y. Qi, N. An, M. Yan, Z. Wang, M. Zhou, S. Yang, *ACS Nano* **2024**, *18*, 19712.
[22] S. Xie, K. Huang, J. Peng, Y. Liu, W. Cao, D. Zhang, X. Li, *Adv. Healthc. Mater.* **2022**, *11*, 2201323.
[23] J. Peng, S. Xie, K. Huang, P. Ran, J. Wei, Z. Zhang, X. Li, *J. Mater. Chem. B* **2022**, *10*, 4189.
[24] J. Zheng, W. Wang, X. Gao, S. Zhao, W. Chen, J. Li, Y.-N. Liu, *Small* **2022**, *18*, 2205252.
[25] X. Yuan, S. Suárez-García, M. De Corato, A. C. Muñoz, I. Pagonabarraga, D. Ruiz-Molina, K. Villa, *Adv. Opt. Mater.* **2024**, *12*, 2303137.
[26] L. Xie, X. Pang, X. Yan, Q. Dai, H. Lin, J. Ye, Y. Cheng, Q. Zhao, X. Ma, X. Zhang, G. Liu, X. Chen, *ACS Nano* **2020**, *14*, 2880.
[27] W. Guo, Y. Wang, K. Zhang, X. Dai, Z. Qiao, Z. Liu, B. Yu, N. Zhao, F.-J. Xu, *Chem. Mater.* **2023**, *35*, 6853.
[28] M. Ussia, M. Urso, S. Kment, T. Fialova, K. Klima, K. Dolezelikova, M. Pumera, *Small* **2022**, *18*, 2200708.
[29] K. Villa, J. Viktorova, J. Plutnar, T. Ruml, L. Hoang, M. Pumera, *Cell Rep. Phys. Sci.* **2020**, *1*, 100181.
[30] M. J. Oh, A. Babeer, Y. Liu, Z. Ren, J. Wu, D. A. Issadore, K. J. Stebe, D. Lee, E. Steager, H. Koo, *ACS Nano* **2022**, *16*, 11998.
[31] G. Hwang, A. J. Paula, E. E. Hunter, Y. Liu, A. Babeer, B. Karabucak, K. Stebe, V. Kumar, E. Steager, H. Koo, *Sci. Robot.* **2019**, *4*, eaaw2388.
[32] A. Khabbazian, L. Kwong, A. Lewis, E. Liu, N. Abdelrazec, A. C. Bakenecker, N. Fontanals, G. Lopez, S. Sánchez, J. M. Lopez, B. Carrillo, M. Farcas, C. Kallweit, A. C. H. Yu, M. Behrad Khamesee, V. Magdanz, *Adv. Healthc. Mater.* **2025**, *14*, 2403423.
[33] P. A. Dalavi, S. S. Murugan, S. Anil, J. Venkatesan, *Biol. Macromol.* **2022**.
[34] Z. Chen, W. Wei, B.-J. Ni, in *Biomass Biofuels Biochem.* (Eds.: H. Ngo, W. Guo, A. Pandey, J.-S. Chang, D.-J. Lee), Elsevier, **2022**, pp. 37–66.
[35] H. H. Tønnesen, J. Karlsen, *Drug Dev. Ind. Pharm.* **2002**, *28*, 621.
[36] Kundu, Anuranjita, Datta, Sriparna, *Int. J. Adv. Pharm. Biol. Chem.* **2012**, *1*, 266.
[37] S. A. Siboro, D. S. Anugrah, K. Ramesh, S.-H. Park, H.-R. Kim, K. T. Lim, *Carbohydr. Polym.* **2021**, *260*, 117779.
[38] V. M. Bilobrov, A. V. Chugaj, V. I. Bessarabov, *Urol. Int.* **2010**, *45*, 326.
[39] A. Khabbazian, M. B. Khamesee, V. Magdanz, *J. Micro-Bio Robot.* **2025**, *21*, 9.
[40] A. Khabbazian, M. B. Khamesee, V. Magdanz, *2024 Int. Conf. Manip. Autom. Robot. Small Scales MARSS* **2024**, 1.
[41] B. J. Barnett, D. S. Stephens, *Am. J. Med. Sci.* **1997**, *314*, 245.
[42] T. Brooks, C. W. Keevil, *Lett. Appl. Microbiol.* **1997**, *24*, 203.
[43] B. Holmes, R. N. Brogden, D. M. Richards, *Drugs* **1985**, *30*, 482.
[44] A. U. Alahakoon, D. D. Jayasena, S. Jung, H. J. Kim, S. H. Kim, C. Jo, *Korean J. Food Sci. Anim. Resour.* **2014**, *34*, 221.
[45] O. Csutak, I. Sarbu, T. Vassu, *J. Food Sci. Eng.* **2013**, *3*, 79.
[46] W. L. Strohmaier, A. Giese, *Urol. Int.* **2001**, *66*, 30.
[47] F. Tentor, B. Grønholt Schrøder, S. Nielsen, L. Schertiger, K. Stærk, T. Emil Andersen, P. Bagi, L. Feldskov Nielsen, *Sci. Rep.* **2022**, *12*, 17818.
[48] W. Pittman, J. O. Moon, L. C. Hamrick, C. E. Cox, J. Clark, S. Childs, D. Pizzuti, J. Fredericks, P. St. Clair, *Am. J. Med.* **1993**, *94*, 101S.
[49] I. S. M. Khalil, Ligtenberg, Leendert-Jan, Magdanz, Veronika, Warle, Michiel, *Commun. Eng.* **2024**, *3*, DOI https://doi.org/10.21203/rs.3.rs-3526473/v1.
[50] L. Matchette, A. Agrawal, T. Pfefer, *Photochem. Photobiol.* **2007**, *83*, 1386.

The table of contents entry should be 50–60 words long and should be written in the present tense. The text should be different from the abstract text.

*Arnima Shrestha[1], Noura Abdelrazec[1], Sirshendu Misra[2], Kartar Singh[3], Michael A. Beazely[3], Sushanta K. Mitra[2], Veronika Magdanz[1]**

Small-scale magnetic alginate robots for localized antibiotic *E.coli* infection treatment

ToC Figure

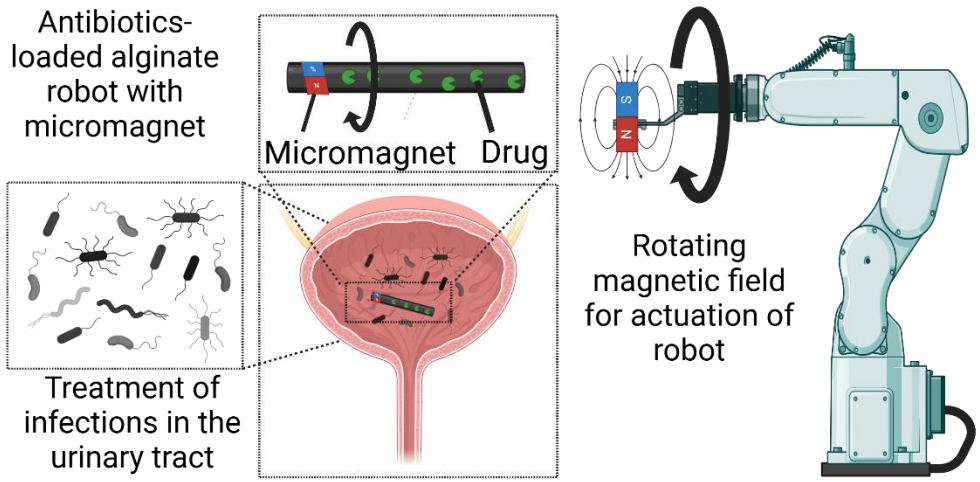

Supporting Information

Small-scale magnetic alginate robots for localized antibiotic *E.coli* infection treatment

*Arnima Shrestha[1], Aarya Bandi[1], Noura Abdelrazec[1], Sirshendu Misra[2], Kartar Singh[3], Michael A. Beazely[3], Sushanta K. Mitra[2], Veronika Magdanz[1]**

Video S1: Magnetic actuation of Alginate filament in human synthetic urine with a permanent magnet rotating at 8 rotations per second inside an ureter-like tube.

Video S2: Alginate filament robot deployment through 14 French catheter into the ex vivo porcine ureter. The rotating permanent is handheld about 10 cm from the robot location. The rotating micromagnet can be seen inside the catheter.

Video S3: Ultrasound detection of moving alginate robot inside the e*x vivo* ureter.

Video S4: Ultrasound detection of moving alginate robot inside the *ex vivo* uretopelvic junction. The ultrasound probe is placed directly on the pig kidney, while the actuator is held 15cm from the kidney to remotely actuate the robot inside the organ.

Video S5: Ultrasound detection of rotating alginate robot inside the *ex vivo* pig kidney (renal pelvis). The inner cavity of the kidney can be seen in the ultrasound image, and the location of the robot is evident due to its flickering signal.

Table S1: Statistical Analysis of E.coli cell concentration at 24,48 and 120h of incubation in synthetic human urine measured by optical density at 600nm at 37 ºC without additives (control), Alginate filaments, NF solution (norfloxacin addition of 10 µg/mL at 0h), and NF loaded alginate filaments (norfloxacin-loaded alginate filaments) performed by one-way ANOVA Tukey test in Origin software.

Sample	Time point	Average E.coli concentration	Standard deviation	Significant difference	R square	Coeff Var	Prob>F
1)Control (E.coli)	24h	1.41x10^8	4.09x10^7	-	-	-	-
2)Alginate filaments		1.28x10^8	6.7x10^7	n.s.	3.6x10^-4	0.41558	0.89813
3)NF solution		5.099x10^7	2.38x10^7	***	0.61448	0.33012	<0.0001
4)NF loaded alginate filaments		2x10^7	8x10^6	***	0.76982	0.34265	<0.0001
Between 3) and 4) at 24h	24h	-	-	***	0.44056	0.50621	<0.0001
1)Control (E.coli)	48h	2.1x10^8	5.7x10^7	-	-	-	-
2)Alginate filaments		2.22x10^8	1.01x10^8	n.s.	0.02839	0.22856	0.40081
3)NF solution		7.15x10^7	3.28x10^7	***	0.69294	0.33196	<0.0001
4)NF loaded alginate filaments		1.43x10^7	7.1x10^6	***	0.88077	0.36574	<0.0001

Between 3) and 4) at 48h	48h	-	-	***	0.61748	0.55695	<0.0001
1)Control (E.coli)	120h	5.95x10^8	1.23x10^8	-	-	-	-
2)Alginate filaments		2.83x10^8	4.58x10^7	***	0.77531	0.20854	<0.0001
3)NF solution		1.01x10^8	3.23x10^7	***	0.90502	0.26666	<0.0001
4)NF loaded alginate filaments		5.76x10^7	3.06x10^7	***	0.91907	0.29674	<0.0001
Between 3) and 4) at 120h	120h	-	-	***	0.41322	0.36171	<0.0001